Composite polyurethane adhesives that debond-on-demand by hysteresis heating in an oscillating magnetic field

Composite polyurethane adhesives that debond-on-demand by hysteresis heating in an oscillating magnetic field.

Sara Salimi,[a] Tahkur S. Babra,[a] Gerald S. Dines,[b] Stephen W. Baskerville,[b] Wayne Hayes,[a] and Barnaby W. Greenland[c*]

[a]Department of Chemistry, University of Reading, Whiteknights, Reading, RG6 6AD UK.
[b]Stanelco RF Technologies Ltd., North Road, Marchwood Industrial Park, Southampton, Hampshire, SO40 4BL UK.
[c]Department of Chemistry, University of Sussex, Falmer Campus, Brighton, Sussex, BN1 9QJ UK

KEYWORDS stimuli responsive, composite, iron particles, adhesive, thermoresponsive, polyurethane, hysteresis heating, oscillating magnetic field.

Abstract

Debond-on-demand adhesives are an emerging industrially important technology, allowing components and materials to be readily separated when required, facilitating recycling. Herein, a composite adhesive has been synthesized that can undergo hysteresis heating to debond-on-demand through direct exposure to an oscillating magnetic field. The adhesive is composed of a polyurethane continuous phase with commercial, unfunctionalized iron oxide particles as the filler (between 1 and 20 wt%). 2 mg of the composite containing 8 wt% iron oxide particles was able to bond various surfaces including glass, wood, aluminium and polyvinyl chloride and support a static load of 100 grams. The composites were fabricated by melt processing which resulted in a relatively inhomogeneous dispersion of particles. The values of the Young's modulus, the ultimate tensile strength, modulus of toughness of the adhesives were comparable to those exhibited by a commercial hot melt adhesive but relatively invariant over the series of composites examined. When subjected to hysteresis heating from an oscillating magnetic field, the rate of temperature increase was dependent on the loading level of Fe_3O_4. Debonding times decreased from approximately 5 minutes to less than 30 seconds exposure to the oscillating magnetic field as the Fe_3O_4 loading level increased from 1 to 20%. These results will help guide the design of new debond-on-demand polymers that can be addressed through exposure to an oscillating magnetic field.

INTRODUCTION:

In recent years there have been significant efforts to produce adhesives with added functionality beyond the ability to securely bond materials.[1,2] For example, adhesives have been produced that can detect specific chemicals,[3] damage,[4] strain,[5] changes in temperature[6] or be activated under specific conditions.[7] Furthermore, responsive adhesives have been produced that exhibit the ability either to heal and rebond two surfaces after fracture or debond-on-demand in response to a specific stimulus.[8–10] A broad range of applications may be envisaged for healable and debondable adhesives, for example, in removable prosthetics,[11] dentures[12–14] or to facilitate recycling of complex multicomponent products including vehicles and mobile phones.

The dynamic nature of specific covalent bonds[15,16] has been successfully used to introduce reversibility into adhesive materials.[9] For example, Michal *et al.* have taken advantage of disulfide bonds to make a reversible shape-memory[17] adhesive whereas Aubert employed Diels-Alder chemistries to generate an adhesive in which the debonding reaction occurs above 90 °C.[18] In addition, Tang *et al.* have produced a dynamic vitrimer based on triazolium salts which proved to be an extremely high strength re-healable adhesive.[19]

A conceptually distinct route to obtain the functionality required to produce debond-on-demand adhesives is to exploit the inherent reversibility of supramolecular bonds.[20,21] Supramolecular materials typically contain relatively low molecular weight species that self-assemble into higher pseudo-crosslinked networks in the solid state.[22] The strength of the supramolecular interactions can be tuned by varying the structure of the supramolecular motifs at the molecular level, which can lead to predictable changes in the response of polymer in the solid state.[23–25] Furthermore, application of an appropriate stimuli results in real time, reversible changes in strength of the supramolecular bonds in the materials which has a dramatic effect on the physical properties (tensile strength/viscosity) of the bulk polymer. For example, hydrogen bonding,[23,26] π-π stacking[27,28] and metal-ligand bonds[8,29,30] have found widespread application as healable and self-healing materials.[27,28,31–33] In these systems, loss of strength caused by damage can be reversed by application of a specific stimulus, for example

pressure, temperature or UV radiation. Recently, our group has produced a rebondable adhesive, which harnessed the thermo-reversibility of a hydrogen bonded polyurethane (PU) but had the added functionality brought by the inclusion of a chemo-responsive monomer in the backbone of the polymer.[34,35] This adhesive underwent multiple bonding/debonding cycles in response to heat and/or force yet could also undergo irreversible reduction of adhesion after depolymerisation on contact with fluoride ions.

A key factor in designing healable and debondable adhesives is the selection of the debonding stimulus because it will constrain the utility of the final adhesive.[36] Hot melt adhesives and their nanocomposites [37] can clearly undergo debonding if the adhesive can be heated to a suitable temperature. However, frequently this is not practical because the bonded region may not be accessible, or the bonded substrates not sufficiently thermally conductive or stable to achieve and maintain the temperatures required to melt the adhesive. In addition, although materials that respond to other stimuli such as UV radiation have been realised,[17] this stimulus can only be used in an adhesive setting if the bonded substrates are transparent at the appropriate wavelengths. For example, Kihara *et al.* took advantage of azobenzene photoisomerization and produced a rebondable adhesive which leaves substrate intact upon debonding as a result of no heat requirement.[38,39] However, the application of this adhesive is limited to situations where at least one of the bonded surfaces is transparent at the appropriate wavelength. This constraint precludes debonding of many common materials by UV/vis radiation (wood, metals, optically opaque polymers).

An alternative method of transferring energy to a material is by the interaction of either ferromagnetic or conductive materials with an oscillating magnetic field (OMF), which can be readily produced by passing a suitable alternating current through an inductor of the correct geometry.[4,40,41] The mechanism of heat generation depends on the nature and size of the material the OMF is interacting with. For conductive non-ferrous/non-magnetic materials, heat is generated by the joule effect related to eddy currents that circulate within the material as a result of field coupling from the OMF directly to the material. The coupling efficiency and heating effect achieved is highly dependent on the frequency and field density of the OMF in relation to specific physical properties and homogeneity of the conductive material being heated. Whereas, when ferromagnetic materials are introduced

into such an OMF then hysteresis heating effects caused by direct magnetic stimulation (excitation) of susceptible particulates will also become applicable. Small ferrous oxide particles such as those used in this work prove difficult to heat effectively due to eddy currents as both the size of the individual particles, their clusters (or groups) and their homogeneity within the material is not conducive to the type of joule heating effect achieved by a typical frequency of application. Heat is produced in this case by nature of the hysteresis effects[42] within each particle and is more dependent on magnetic field strength and field density. The hysteresis effect causes friction heating as the particles are repeatedly taken through magnetic hysteresis loops.[4,43]

Induction heating from an OMF is used widely on an industrial scale for welding and melting metals. Also, induction sealing has been extensively used for six decades for hermetic sealing of different thermoplastic packages with no effect on the contents.[44] Adzima *et al.* have investigated the use of induction heating to provide the energy for healing Diels-Alder crosslinked networks.[41] More recently, Ahmed *et al.* produced a multifunctional healable material through induction heating of a polyvinyl acetate nanocomposite.[4]

It would be possible to harness the energy transfer of an OMF to iron oxide particles within PU thermoplastic adhesive[45] to produce a debond-on-demand composite adhesive (**Scheme 1**).[46] OMFs, particularly those of the frequency domain used in this work, do not have a heating effect on many commonly bonded materials such as wood, plastic and glass. This overcomes problems associated with melting or degrading the bonded substrates when attempting to heat a thermo-responsive adhesive to its melting

temperature.

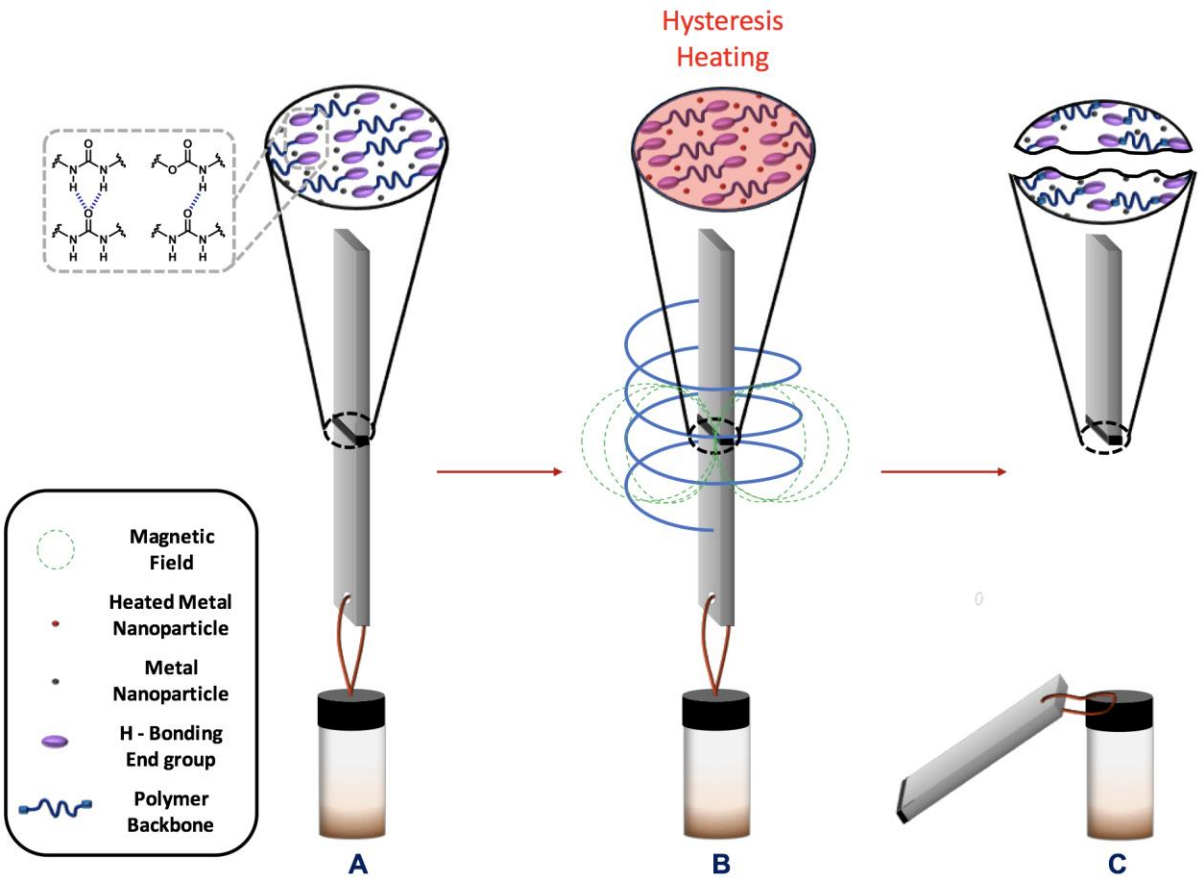

Scheme 1: Concept schematic of a healable and OMF debondable Fe_3O_4 composite adhesive: A) the PU-composite bonding two substrates; B) application of OMF from an inductor which heats the adhesive via energy dissipated from hysteresis loss in Fe_3O_4 particles and C) the supramolecular bonds in the PU network weakened by the heat, allowing facile debonding of the substrates.

Herein, we describe the synthesis of the first composite adhesive that can be heated and therefore readily debonded on exposure to an OMF. This is achieved by the addition of iron oxide particles to the PU, which are known to be heated efficiently under OMF conditions.[47] We show that the composite adhesive can bond a range of substrates including glass, wood, aluminum and polyvinyl chloride (PVC), and can be rapidly heated to facilitate debonding when placed in an OMF.

RESULTS and DISCUSSION

Design and synthesis of the continuous PU phase of the adhesive

PU adhesive **1** was synthesized from 3 components; a hydrogenated hydroxyl-terminated polyolefin diol **2** (Krasol HLBH-P2000), methylenebis(phenyl isocyanate) (MDI) **3** to afford the pre-polymer in the absence of solvent[48] (**4**) which was end-capped by the addition of 4-(2-aminoethyl)morpholine (**5**) (Scheme 2). The chemical composition of the polymer was selected because we have previously demonstrated closely related materials to be non-toxic and to be adhesive to biological surfaces.[33] The polymer was isolated in a yield of 80% after precipitation into methanol (10.3 $kg.mol^{-1}$, Đ=1.63).

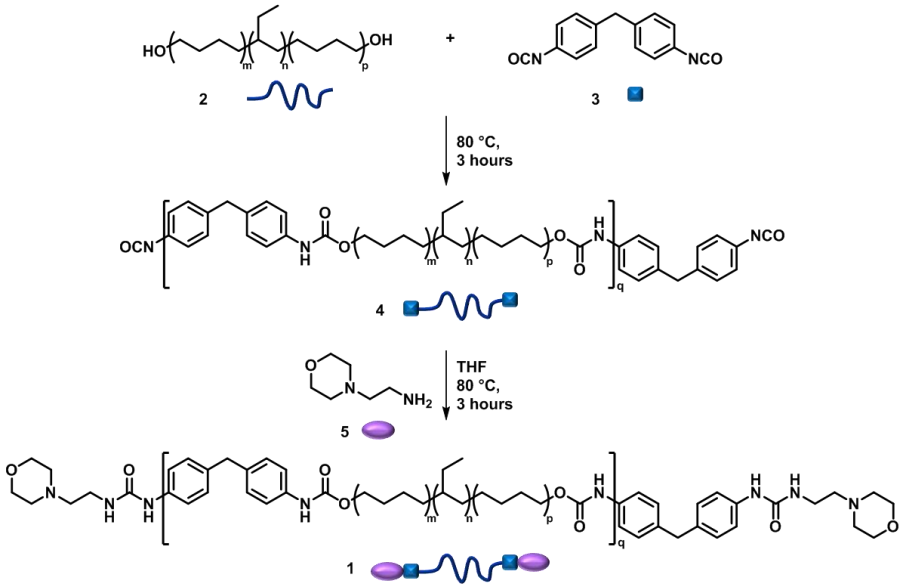

Scheme 2: synthesis of the polyurethane (**PU1**). Each chemical structure is also denoted schematically (ratio of OH:NCO = 1:1).

Films suitable for tensile testing were cast from THF in PTFE moulds (15 × 15 cm) and dried slowly under vacuum for 18 h. Residual solvent could not be detected by either ^{1}H NMR spectroscopy or DSC analysis (see supporting information **Figures S1** and **Figure S2** respectively). Variable temperature analysis of the polymer by ^{1}H NMR spectroscopy in solution and IR spectroscopy in the solid state revealed the presence of the expected hydrogen bonding interactions between the urea and urethane components (see SI **Figures S3** and **Figure S5**).

Composite synthesis and analysis

A series of composites were produced from **PU1** which differed in the quantity of iron oxide particles incorporated (up to 20 wt%). Each composite was formulated by melt processing. The required wt% of iron oxide particles was hand mixed with a known quantity of **PU1** above the melting temperature of the polymer (100 °C, see SI Figure S14) to produce six composite samples which varied by the filler loading level (1, 5, 8, 12, 16 and 20 wt%).

Initial adhesion studies were carried out by applying a circular sample of the 8 wt % composite (*ca*. 2 mg, 2 mm diameter, 0.6 mm thickness) to the surface of untreated sample of different substrates: wood, aluminum, PVC and glass. Then bonding two such sample surfaces together in a lap joint form. The prepared samples were placed on a preheated hot plate at 80 °C for 3 minutes on each side. After cooling to room temperature, all the samples had bonded securely, and they could be handled without breaking. Regardless of the bonded substrate material, the composite showed the ability to hold a static load of 100 g (**Figure 1**).

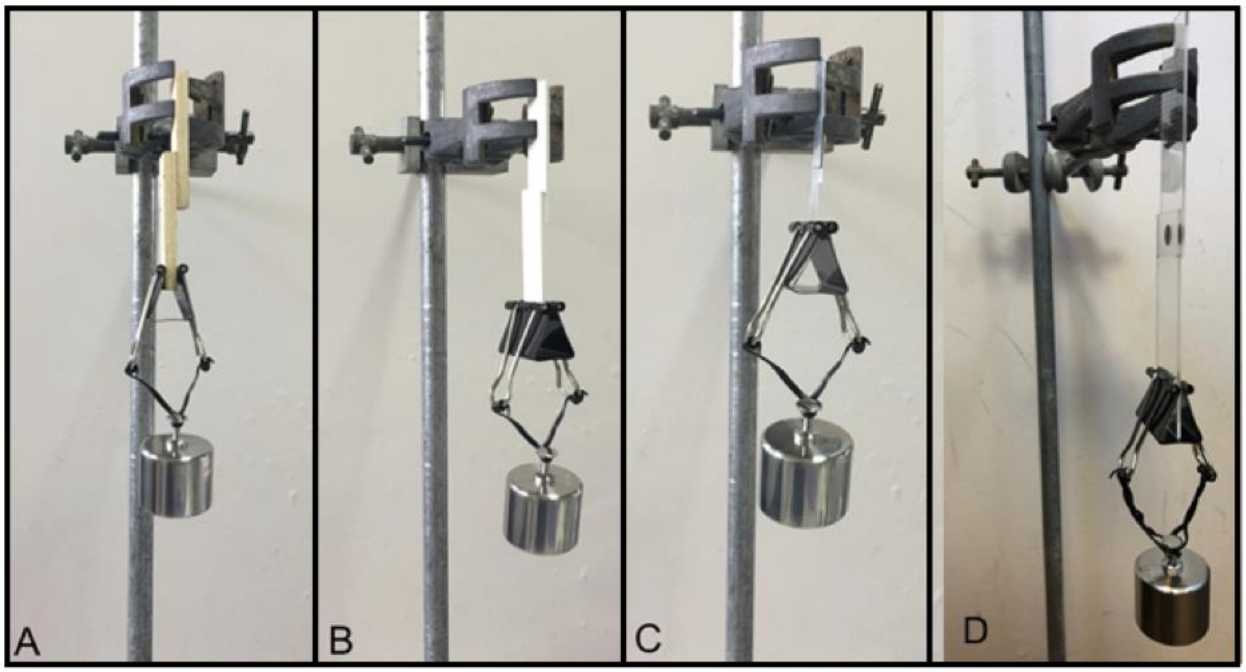

Figure 1: Substrates (A) wood, (B) PVC, (C) aluminium and (D) glass bonded by 2 mg of the 8% composite supporting a static 100 g load. Surfaces were not surface treated prior to bonding.

Visual inspection of the adhered glass slides showed that the iron oxide particles were not homogeneously dispersed throughout the PU in the bonded samples.[31] **Figure 2** shows the images taken of each wt% composite as viewed through the adhered glass slide. During the bonding process the polymer has flowed outward resulting in a final diameter of approximately 7 mm (starting diameter = 2 mm) (See SI **Figure S7**), accounting for the spoke-like distribution of the particles. It can be seen that the samples all contain dense, black, highly aggregated regions (approximately 20 - 80 microns particle clusters) and cloudy-looking regions where the particles are more evenly dispersed. The area covered by the particles, whether aggregated or finely dispersed was determined by comparison of the dark and light regions by image analysis (**Table 1**).

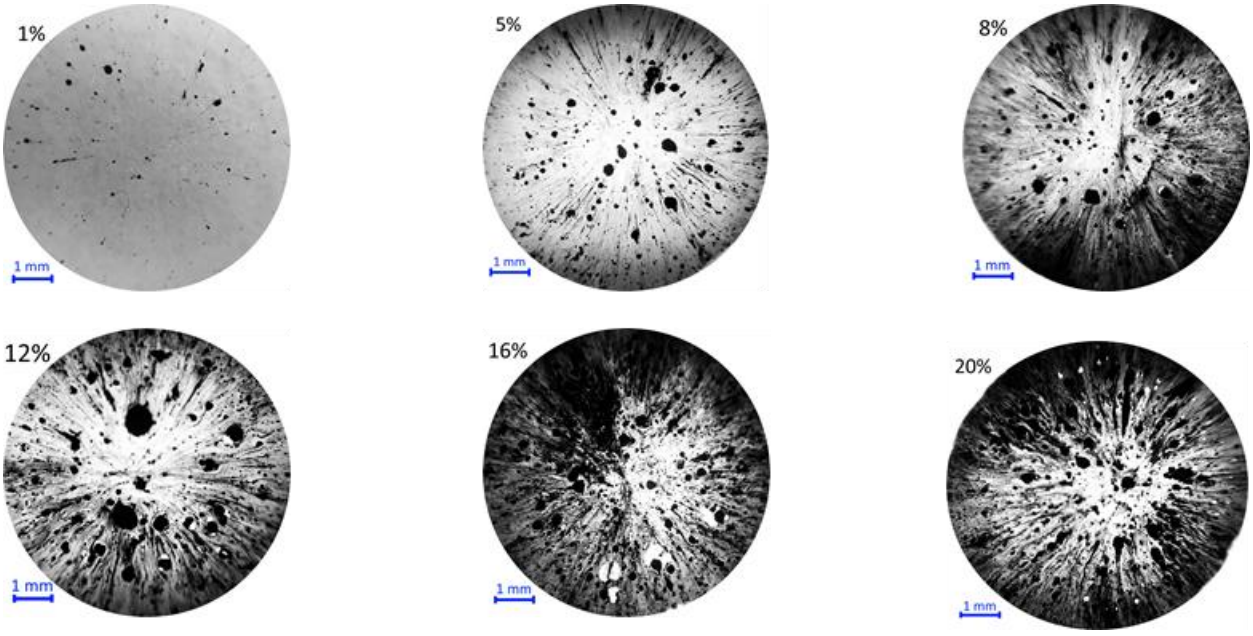

Figure 2: Black and white pictures of the composites taken with macro lens to investigate Fe_3O_4 particle aggregation at each wt% loading level.

Table 1: The formulated iron oxide particle loading level and the coverage of particles (from Figure 2) for each composite as determined from the images of the adhesives using *ImageJ*.

Formulated loading level (wt%)	1.0	5.0	8.0	12.0	16.0	20.0
Area coverage of particles (%)	1.2	6.3	13.1	12.6	21.0	24.0

The deviation between the area covered by the iron oxide particles and the known loading may be accounted for by the low energy formulation of the composite by hand mixing which did not efficiently separate the highly magnetic iron particles.[49,50] Thus, the dense areas contain particles in three dimensions, but they are only observed in two dimensions in the processed image of the adhesives. Indeed, the fabrication of adhesives with higher filler loading levels was not attempted as a consequence of the difficultly in dispersing the particles using this low energy formulation technique even at 20 wt% Fe_3O_4. However, the inhomogeneity of the composites clearly did not prevent adhesion (**Figure 1**) and, therefore, attention turned towards quantifying the effect of the level of filler on both bond strength and potential debond-on-demand properties of the adhesive.

Adhesive testing

Each composite (1-20 wt% filler) and the pristine **PU1** that did not contain Fe_3O_4 were used to bond two glass slides together, as described during the imaging experiments. We selected the commercial adhesive, Tecbond™ 484-9900, which is delivered by a hot glue gun, as a typical commercial example to compare our novel composite adhesives to in terms of materials properties. The bonding properties of the adhesives were measured in the lap sheer geometry. These data are summarized in **Figure 3** which shows the ultimate tensile strength (UTS), Young's modulus and modulus of toughness for each of the samples (See SI **Figure S9** for representative stress-strain plots).

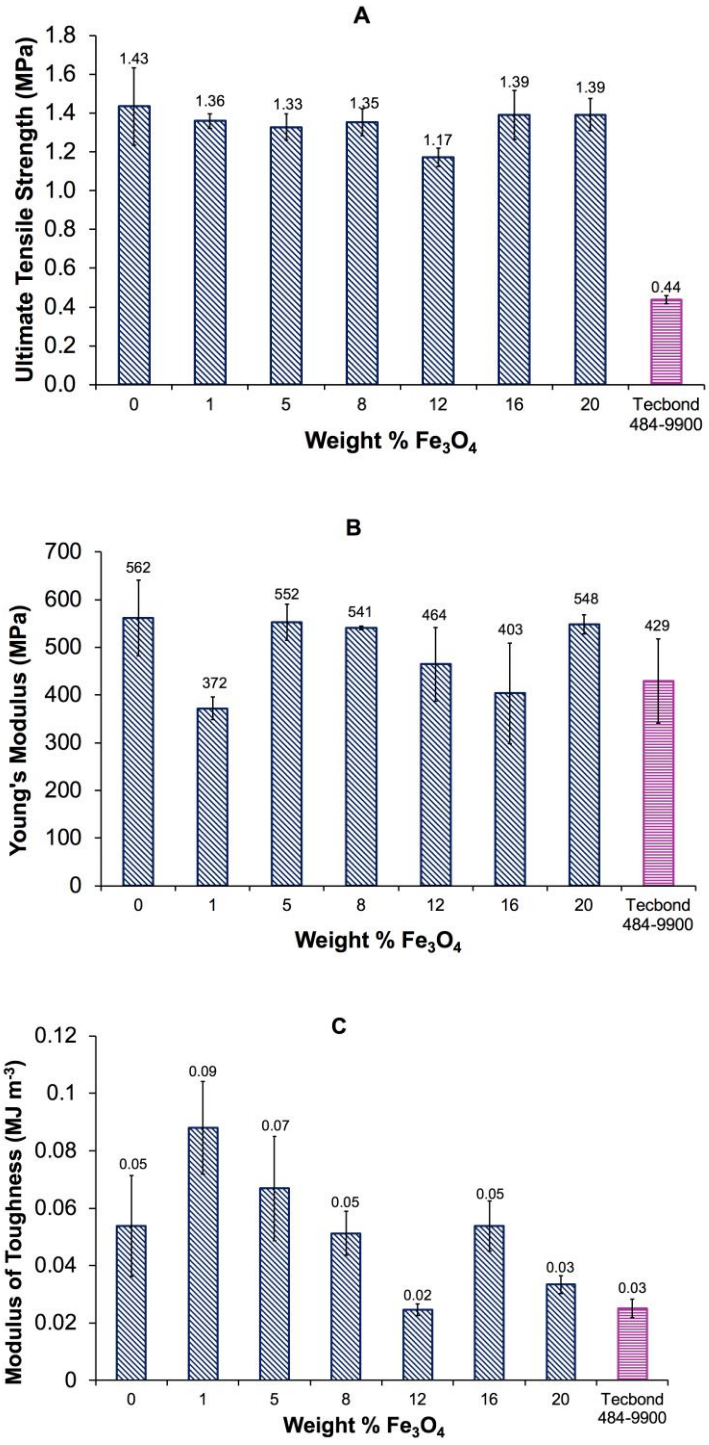

Figure 3: Lap shear tensile data for composites containing varying quantities of iron oxide particles compared with a commercially available hot melt adhesive. Mean values are reported above each bar. Errors are the standard deviations from the mean of 3 repetitions.

No significant differences were observed in the UTS, Youngs Modulus or modulus of toughness between **PU1** and each of the different wt% composites which indicate that although the presence of filler does not inhibit the adhesion ability of the PU, it does not significantly improve the mechanical properties of the materials as often observed for inorganic fillers.[51] This may be accounted for by the inhomogeneity of the dispersion of the filler (**Figure 2**), but may also be as a consequence of the lack of molecular scale interaction between the filler and PU. A similar result was obtained by Hayes and co-workers when studying healable materials containing gold nanoparticles.[52] In this work, enhanced mechanical properties were only observed in the materials when specific recognition motifs were installed to allow supramolecular interactions between the filler and the continuous phase. Gratifyingly, all the novel adhesives performed comparably to the commercial sample, with the 1% Fe_3O_4 exhibited an improvement in UTS and modulus of toughness of 210% and 67%, respectively.

Hysteresis Heating Experiments

After establishing the adhesive nature of the composites, their response to hysteresis heating conditions was investigated. A circular sample (*ca.* 2 mg) of each composite was placed on a petri dish with a sample of **PU1** in the middle for comparation (**Figure 4 A1**). The petri dish was placed on top of the OMF generating inductor (**Figure 4 A2**) and the change in temperature of the samples was monitored using a thermal camera. The images show the temperature change over the first minute of heating (**Figure 4: B1** to **B4**).

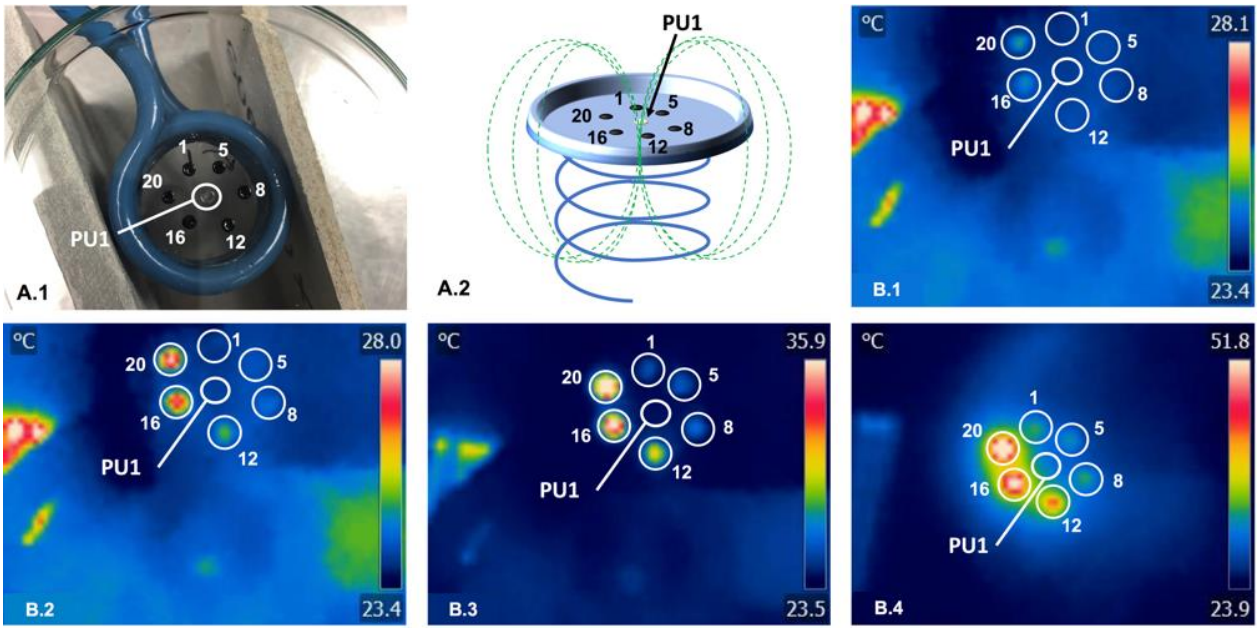

Figure 4: Photograph (A1) and schematic (A2) of the composite samples (1 to 20 wt%) placed in a ring around a sample of **PU1** above the inductor used to produce the OMF. (B1 to B4) Thermal images of the samples showing the temperature change between 5 seconds and 1 minute of exposure to the OMF.

Analysis of the thermal images show the sample of **PU1** that does not contain Fe_3O_4 is not heated in the presence of the OMF. In this heating geometry, where the samples are positioned above the inductor, the 20 wt% sample was heated to approximately 50 °C in one minute, whereas the temperature of the composite samples containing less than 8 wt% Fe_3O_4 were heated to approximately 27 °C, which was only just above ambient (23 °C) over the same time period.

Hysteresis Heating Debonding Experiments

In order to study the debond-on-demand properties of the composite adhesives, an industry standard dog bone-shaped tensile strength test piece was halved, the cut surfaces were sanded and then re-bonded in butt joint form using 2 mg of the adhesive by heating at 60 °C for 30 mins in an oven. The butt joint form was used in order to effectively eliminate any vertical sheer 'friction' load from the test results. After cooling, the dog bones were suspended by their top end with the butt bonded central region positioned

in the centre of a three-turn solenoidal inductor and a 25 g weight was hung from the bottom end (**Figure 5**).

Figure 5: Image showing the sample setting for the OMF initiated debonding experiments.

Figure 6 shows the time required for bonding failure for composite adhesive samples containing increasing wt% of particles. It can be seen that among adhesives containing between 1 and 20 wt% iron oxide particles, OMF induced debonding occurred at decreasing times (307.5 and 22.5 seconds for 1 and 20 wt%, respectively). A greater loading of particles converts an increasing amount of energy from the OMF to heat, reducing time required to reach the temperature necessary for the sample to debond under the force of gravity.

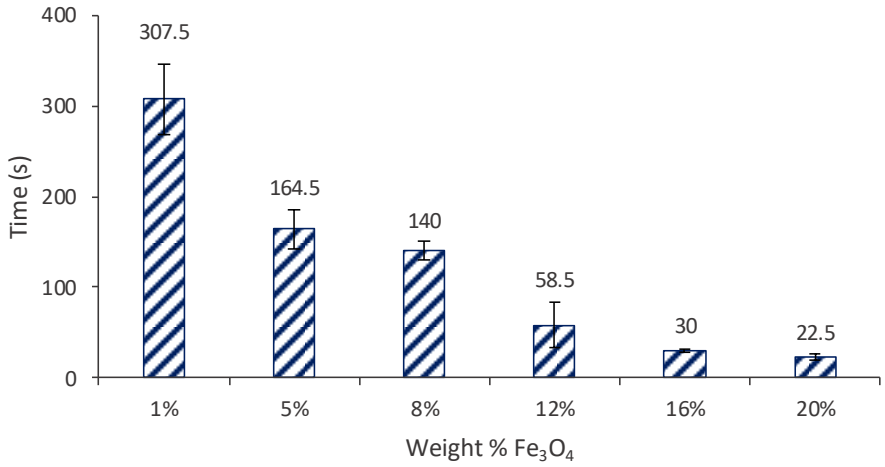

Figure 6: Debonding time for the composite adhesives under hysteresis heating condition. Mean values are reported above each bar. Errors are the standard deviations from the mean of 2 repetitions.

Conclusion

In conclusion, a PU-based adhesive was synthesized that could adhere to different substrates including wood, aluminum, glass and PVC under thermal conditions. Dispersion of unmodified Fe_3O_4 particles up to 20 wt% was achieved by a simple melt processing protocol. Although in-homogeneously dispersed, the composite adhesives exhibited bond strengths comparable to a commercial hot melt adhesive. The composites could be heated by interaction with an OMF generated by a three-turn solenoidal inductor. The rate of heating derived from a constant source field was dependent on the loading level of iron particles. Debond-on-demand tests were carried out by placing the butt-joint bonded section of a dogbone sample in the center of the inductor and applying a 25 g weight. The time taken to debond the system under the force of gravity was inversely related to the loading level of the filler, reducing from over 5 minutes to less than 30 seconds as the filler loading increased from 1 to 20 wt%. This work shows that OMFs may be used to heat iron oxide composite adhesives in order to facilitate joint debonding. However, it is worth noting that this method of heating may be deemed less suitable when applied to joints containing other ferromagnetic or conductive materials, due to the fact that those joint materials may heat preferentially (compared to the composite adhesive) when exposed to the OMF. Although such preferential heating could lead to softening and debonding effects, it would most probably be due to, or directly affected by, thermal

conduction from the bonded substrate, as opposed to being entirely due to slective heating of the composite particulate. We are currently investigating how to improve dispersion of the particles in efforts to improve the strength of the adhesive without compromising the rapid heating and debonding behavior of the system through non-invasive interaction with an OMF.

Supporting Information

The Supporting Information is available free of charge:
Characterization data (NMR, DSC, IR, VT-IR, GPC, Rheology, typical tensile testing data plots)

AUTHOR INFORMATION

Corresponding Author

* b.w.greenland@sussex.ac.uk

Author Contributions

The manuscript was written through contributions of all of the authors.

Notes

GSD and SWB work for Stanelco RF Technologies Ltd who manufacture various types of industrial heating equipment utilising RF technology.

ACKNOWLEDGMENT

The authors would like to thank Stanelco RF Technologies for use of their induction generator and facilities. We are thankful to Davood Salimi and Mahboubeh Shabani for funding SS and to the University of Reading for part funding a PhD studentship for TSB. We are also grateful to the University of Reading for access to instrumentation in the Chemical Analysis Facility and to Cray Valley for the supply of Krasol HLBH-P2000.

EXPERIMENTAL:

Materials: 4,4′-Methylenebis(phenyl isocyanate) (MDI) (Sigma-Aldrich, 98%), 4-(2-aminoethyl)morpholine (Alfa Aesar, 98+%), Iron (III) oxide nanoparticles < 50 nm (BET)

(Sigma Aldrich) was used as received. Tetrahydrofuran (THF, 0.025% BHT) (Fisher Scientific) was distilled from sodium/benzophenone under nitrogen to obtain anhydrous THF. Krasol HLBH-P2000 was kindly supplied by Cray Valley and was dried overnight in vacuum oven at 100 °C at 900 mbar prior to use. The dog-bone shaped plastic substrate for OMF testing were supplied by Biome Bioplastics Ltd (reference HT90), a sister division of Stanelco RF Technologies Ltd.

Methods: ^{1}H and ^{13}C NMR spectra were collected using a Bruker Ultrashield™ Plus 400. Samples were prepared in $CDCl_3$ with 0.5 mg of polymers in 0.7 mL solvent. The residual proton peak for the solvent was set to 7.26 ppm. Polymer molecular weight data were obtained using gel permeation chromatography (GPC). This was conducted using an Agilent Technologies 1260 Infinity system equipped with a refractive index (RI) detector and two Agilent PLgel 5 µm MIXED-D 300×7.5 mm columns in series calibrated with low Đ polystyrene standard and eluting with analytical grade THF (2 mg/mL) with butylated hydroxytoluene (BHT). Samples were dissolved in the same solvent (2 mg/mL) and filtered through a syringe filter (0.2 µm). Data were processed using standard Agilent GPC/SEC software in comparison to polystyrene standards. Differential scanning calorimetry (DSC) experiments were carried out using Tzero aluminum pans with TA Instruments Q2000. 0.7 mg of each polymer film was heated from -80 °C to 200 °C at a rate of 10 °C /min under an N_2 atmosphere. Both variable temperature IR and room temperature IR spectra were collected using PerkinElmer Spectrum 100 FT-IR Spectrometer. Tensile test data were recorded using AML instruments™ single column tensiometer while the samples were stretched at the speed of 1 mm/min.

Synthesis of the PU1:[24,33] Krasol™ HLBH-P2000 (12.6 g, 6.00 mmol) and MDI **(**3.15 g, 12.60 mmol) were heated to 80 °C for 3 hours under nitrogen to form the pre-polymer. The mixture was cooled to room temperature and dissolved in anhydrous THF. 4-(2-aminoethyl)morpholine (3.59 g, 13.20 mmol) was added to the solution and the reaction reflux at 80 °C under N_2 for 3 hours. THF was then removed *in vacuo*. The polymer dissolved in chloroform and then precipitated in methanol. The solvent was decanted, and the precipitate was dissolved in THF and evaporated *in vacuo* (13.7 g, 80%).

^{1}H NMR (400 MHz, $CDCl_3$) δ: 7.15 – 7.05 (aromatic H), 6.6 (urethane NH), 5.4 - 5.2 (urea NH), 4.25 – 4.01 (diol CH_2**CH_2**O), 3.4 – 3.3 (end group NH**CH_2**CH_2), 3.7 – 3.6 (end group O**CH_2**CH_2), 3.9 – 3.8 (MDI C**CH_2**C), 2.5 – 2.4 (end group CH_2**CH_2**N), 2.1 – 0.6 (diol chain H). ^{13}C NMR (400 MHz, $CDCl_3$) δ: 136.11, 129.7-129.41, 121.77, 118.87, 77.80 – 76.81, 66.92, 53.34, 40.61, 38.87 – 37.87, 36.81 – 36.11, 34.10 – 33.24, 30.67 29.77, 27.10 – 25.87, 11.1 – 10.3, , GPC (SI **Figure S13**) M_n= 10.3 kg.mol^{-1}, Đ=1.63.

Casting of PU films: The polymer was dissolved in THF at room temperature and poured into a 15 cm x 15 cm PTFE mould and left at room temperature for 5 hours during which time a tacky film formed. The mould was then placed into a vacuum oven at 40 ºC and 800 mbar overnight for complete removal of the residual solvent. After cooling down to room temperature the homogeneous, bubble-free polymer film was easily removed in one piece from the mould.

Composite formation: Six composite samples which varied by the filler loading level (1, 5, 8, 12, 16 and 20 wt%) were produced using 1.0 g of the **PU1** film. The film was placed on a PTFE plate and heated to 100 °C on a preheated hot plate. When the polymer viscosity decreased sufficiently to allow mixing of the iron oxide (See SI Figure S14 for rheology data), the appropriate amount of iron oxide was added and stirred until further mixing did not visually change the appearance of the composite.

Lap shear sample preparation: Using a 2mm circle cutter, ~ 2 mg of each composite film was cut and sandwiched between two glass slides to adhere them (total weight of 10 samples = 21 mg). The glass slides were secured using paperdog clips to minimize movement during adhesion. The samples to be bonded were placed on a preheated hot plate at 80 °C for 3 minutes on each side. After cooling down to room temperature, the paper clips were removed, and the samples were ready for testing (SI **Figure S6**).

Lap Shear: The bonded glass slides were placed between the grips of the tensiometer and separated at a speed of 1 mm/min while the change in stress versus changes in strain was recorded.

Dog-bone sample preparation: The dog-bone shaped plastic pieces were cut in half and the new surfaces sanded until smooth to the touch. Using a 2mm circle cutter, ~ 2 mg of

each composite was sandwiched between two pieces to re-attach the sides. The pieces were then secured using bulldog clips. Samples were then put inside an oven at 60 °C for 30 mins. After cooling down to room temperature, the bulldog clips were removed, and the samples were ready for testing (SI **Figure S8**).

Imaging and image processing the composites: After preparing the samples, a clip macro lens was attached to an iPhone 8 camera. The samples were backlit to increase the image contrast and black and white images were obtained for each sample. Images were then processed using *ImageJ* software to assess the ratio of black (iron oxide particles) to white (**PU1**).

Tecbond 484-9900 testing: A glue gun was used to continuously extrude Tecbond 484-9900 on a PTFE plate with the same thickness as our composite films (appx 0.8 mm). A circle with 2 mm diameter was cut using a die and placed between two glass slides which were fixed with 2 paper clips to minimise movement during adhesion (weight of 10 adhesive samples = 26 mg). Samples were place on a pre-heated hot plate (80 °C) for 3 min before turning and heating for a further 3 min. After cooling to room temperature the paper clips were removed prior to stress/strain testing as described above.

OMF debonding experiment: A prepared dog-bone shaped sample was suspended vertically through the axis of the solenoidal inductor (**Figure 5**) and a 25 g weight was attached to it. An OMF (as specified below) was applied and the time required for the adhesive to fail was recorded.

OMF generator specification: The OMF generator used (Model RFP-7500-0.4) had a maximum rating of 7.5kW, and was operating at 308 kHz with a maximum of 800A AC current passing through a short-length solenoidal induction coil (L= 2.9 cm, d = 3.5 cm, number of turns = 3). In this experimental setting a magnetic field strength of 5000-10000 $A.m^{-1}$ was calculated to have been generated in the centre of the solenoidal inductor.

REFERENCES

[1] A.H. Hofman, I.A. van Hees, J. Yang, M. Kamperman, Bioinspired Underwater Adhesives by Using the Supramolecular Toolbox, Adv. Mater. 30 (2018) 1704640. doi:10.1002/adma.201704640.

[2] C. Heinzmann, C. Weder, L.M. De Espinosa, Supramolecular polymer adhesives: Advanced materials inspired by nature, Chem. Soc. Rev. 45 (2016) 342–358. doi:10.1039/c5cs00477b.

[3] W. Tan, L. Zhang, W. Shen, Low-Cost Chemical-Responsive Adhesive Sensing Chips, ACS Appl. Mater. Interfaces. 9 (2017) 42366–42371. doi:10.1021/acsami.7b14122.

[4] A.S. Ahmed, R. V. Ramanujan, Magnetic Field Triggered Multicycle Damage Sensing and Self Healing, Sci. Rep. 5 (2015) 13773. doi:10.1038/srep13773.

[5] M. Liao, P. Wan, J. Wen, M. Gong, X. Wu, Y. Wang, R. Shi, L. Zhang, Wearable, Healable, and Adhesive Epidermal Sensors Assembled from Mussel-Inspired Conductive Hybrid Hydrogel Framework, Adv. Funct. Mater. 27 (2017) 1703852. doi:10.1002/adfm.201703852.

[6] S.B. Khan, M.T.S. Chani, K.S. Karimov, A.M. Asiri, M. Bashir, R. Tariq, Humidity and temperature sensing properties of copper oxide-Si-adhesive nanocomposite, Talanta. 120 (2014) 443–449. doi:10.1016/j.talanta.2013.11.089.

[7] S. Fujii, S. Sawada, S. Nakayama, M. Kappl, K. Ueno, K. Shitajima, H.-J. Butt, Y. Nakamura, Pressure-sensitive adhesive powder, Mater. Horiz. 3 (2016) 47–52. doi:10.1039/C5MH00203F.

[8] C. Heinzmann, S. Coulibaly, A. Roulin, G.L. Fiore, C. Weder, Light-induced bonding and debonding with supramolecular adhesives, ACS Appl. Mater. Interfaces. 6 (2014) 4713–4719. doi:10.1021/am405302z.

[9] A.M. Asadirad, S. Boutault, Z. Erno, N.R. Branda, Controlling a polymer adhesive using light and a molecular switch, J. Am. Chem. Soc. 136 (2014) 3024–3027. doi:10.1021/ja500496n.

[10] J. Liu, Y. Tan, C, S, O.A. Scherman, Dynamic Interfacial Adhesion through Cucurbit [n] uril Molecular Recognition, Angew. Chem. 130 (2018). doi:10.1002/anie.201800775.

[11] M.L.B. Palacio, B. Bhushan, S.R. Schricker, Gecko-inspired fibril nanostructures for

reversible adhesion in biomedical applications, Mater. Lett. 92 (2013) 409–412. doi:10.1016/j.matlet.2012.11.023.

[12] A.O. Matos, J.O. Costa, T. Beline, E.S. Ogawa, W.G. Assunção, M.F. Mesquita, R.X. Consani, V.A. Barão, Effect of Disinfection on the Bond Strength between Denture Teeth and Microwave-Cured Acrylic Resin Denture Base, J. Prosthodont. 27 (2018) 169–176. doi:10.1111/jopr.12468.

[13] S.K. Gill, N. Roohpour, Y. An, J.E. Gautrot, P.D. Topham, B.J. Tighe, Hydrophobic and hydrophilic effects on water structuring and adhesion in denture adhesives, J. Biomed. Mater. Res. - Part A. 106 (2018) 1355–1362. doi:10.1002/jbm.a.36341.

[14] S.K. Gill, N. Roohpour, P.D. Topham, B.J. Tighe, Tuneable denture adhesives using biomimetic principles for enhanced tissue adhesion in moist environments, Acta Biomater. 63 (2017) 326–335. doi:10.1016/j.actbio.2017.09.004.

[15] S.J. Rowan, S.J. Cantrill, G.R.L. Cousins, J.K.M. Sanders, J.F. Stoddart, Dynamic Covalent Chemistry, Angew. Chemie Int. Ed. 41 (2002) 898–952. doi:10.1002/1521-3773.

[16] J. Dahlke, S. Zechel, M.D. Hager, U.S. Schubert, How to Design a Self-Healing Polymer: General Concepts of Dynamic Covalent Bonds and Their Application for Intrinsic Healable Materials, Adv. Mater. Interfaces. (2018) 1800051. doi:10.1002/admi.201800051.

[17] B.T. Michal, E.J. Spencer, S.J. Rowan, Stimuli-Responsive Reversible Two-Level Adhesion from a Structurally Dynamic Shape-Memory Polymer, ACS Appl. Mater. Interfaces. 8 (2016) 11041–11049. doi:10.1021/acsami.6b01251.

[18] J.H. Aubert, Thermally removable epoxy adhesives incorporating thermally reversible Diels-Alder adducts, J. Adhes. 79 (2003) 609–616. doi:10.1080/00218460309540.

[19] J. Tang, L. Wan, Y. Zhou, H. Pan, F. Huang, Strong and efficient self-healing adhesives based on dynamic quaternization cross-links, J. Mater. Chem. A. 5 (2017) 21169–21177. doi:10.1039/c7ta06650c.

[20] L.R. Hart, J.L. Harries, B.W. Greenland, H.M. Colquhoun, W. Hayes, Healable supramolecular polymers, Polym. Chem. 4 (2013) 4860–4870. doi:10.1039/c3py00081h.

[21] T. Aida, E.W. Meijer, S.I. Stupp, Functional supramolecular polymers, Science (80-.). 335 (2012) 813–817. doi:10.1126/science.1205962.

[22] Y. Yang, M.W. Urban, Self-Healing of Polymers via Supramolecular Chemistry, Adv. Mater. Interfaces. (2018) 1800384. doi:10.1002/admi.201800384.

[23] A.W. Bosman, R.P. Sijbesma, E.W. Meijer, Supramolecular polymers at work, Mater. Today. 7 (2004) 34–39. doi:10.1016/S1369-7021(04)00187-7.

[24] P.J. Woodward, D.H. Merino, B.W. Greenland, I.W. Hamley, Z. Light, A.T. Slark, W. Hayes, Hydrogen bonded supramolecular elastomers: Correlating hydrogen bonding strength with morphology and rheology, Macromolecules. 43 (2010) 2512–2517. doi:10.1021/ma9027646.

[25] D.H. Merino, A. Feula, K. Melia, A.T. Slark, I. Giannakopoulos, C.R. Siviour, C.P. Buckley, B.W. Greenland, D. Liu, Y. Gan, P.J.F. Harris, A.M. Chippindale, I.W. Hamley, W. Hayes, A systematic study of the effect of the hard end-group composition on the microphase separation, thermal and mechanical properties of supramolecular polyurethanes, Polym. (United Kingdom). 107 (2016) 368–378. doi:10.1016/j.polymer.2016.07.029.

[26] P. Cordier, F. Tournilhac, C. Soulié-Ziakovic, L. Leibler, Self-healing and thermoreversible rubber from supramolecular assembly, Nature. 451 (2008) 977–980. doi:10.1038/nature06669.

[27] S. Burattini, B.W. Greenland, D.H. Merino, W. Weng, J. Seppala, H.M. Colquhoun, W. Hayes, M.E. Mackay, I.W. Hamley, S.J. Rowan, A Healable Supramolecular Polymer Blend Based on Aromatic π - π Stacking and Hydrogen-Bonding Interactions, J. Am. Chem. Soc. 132 (2010) 12051–12058. doi:10.1021/ja104446r.

[28] S. Burattini, H.M. Colquhoun, J. Fox, D. Friedmann, B.W. Greenland, P.J.F. Harris, W. Hayes, M.E. Mackay, S.J. Rowan, A self-repairing, supramolecular polymer

system: healability as a consequence of donor–acceptor π–π stacking interactions, Chem. Commun. (2009) 6717–6719. doi:10.1039/b910648k.

[29] J.B. Beck, J.M. Ineman, S.J. Rowan, Metal/ligand-induced formation of metallo-supramolecular polymers, Macromolecules. 38 (2005) 5060–5068. doi:10.1021/ma050369e.

[30] M. Burnworth, L. Tang, J.R. Kumpfer, A.J. Duncan, F.L. Beyer, G.L. Fiore, S.J. Rowan, C. Weder, Optically healable supramolecular polymers, Nature. 472 (2011) 334–337. doi:10.1038/nature09963.

[31] R. Vaiyapuri, B.W. Greenland, H.M. Colquhoun, J.M. Elliott, W. Hayes, Evolution of supramolecular healable composites: A minireview, Polym. Int. 63 (2014) 933–942. doi:10.1002/pi.4685.

[32] S. Burattini, B.W. Greenland, D. Chappell, H.M. Colquhoun, W. Hayes, Healable polymeric materials: a tutorial review, Chem. Soc. Rev. 39 (2010) 1973. doi:10.1039/b904502n.

[33] A. Feula, X. Tang, I. Giannakopoulos, A.M. Chippindale, I.W. Hamley, F. Greco, C. Paul Buckley, C.R. Siviour, W. Hayes, C.P. Buckley, C.R. Siviour, W. Hayes, An adhesive elastomeric supramolecular polyurethane healable at body temperature, Chem. Sci. 7 (2016) 4291–4300. doi:10.1039/C5SC04864H.

[34] T.S. Babra, A. Trivedi, C.N. Warriner, N. Bazin, D. Castiglione, C. Sivour, W. Hayes, B.W. Greenland, Fluoride degradable and thermally debondable polyurethane based adhesive, Polym. Chem. 8 (2017) 7207–7216. doi:10.1039/C7PY01653K.

[35] T.S. Babra, M. Wood, J.S. Godleman, S. Salimi, C. Warriner, N. Bazin, C.R. Siviour, I.W. Hamley, W. Hayes, B.W. Greenland, Fluoride-responsive debond on demand adhesives: Manipulating polymer crystallinity and hydrogen bonding to optimise adhesion strength at low bonding temperatures, Eur. Polym. J. 119 (2019) 260–271. doi:10.1016/j.eurpolymj.2019.07.038.

[36] B.K. Storm, M. Gwisdalski, D. Lindvang, M. Rann, Investigation of degradation of structural adhesives under influence of chemicals, Macromol. Symp. 225 (2005)

205–219. doi:10.1002/masy.200550716.

[37] G. Otorgust, H. Dodiuk, S. Kenig, R. Tenne, Important insights into polyurethane nanocomposite-adhesives; a comparative study between INT-WS 2 and CNT, Eur. Polym. J. 89 (2017) 281–300. doi:10.1016/j.eurpolymj.2017.02.027.

[38] S. Ito, H. Akiyama, M. Mori, M. Yoshida, H. Kihara, Azobenzene-Containing Triblock Copolymer Adhesive Based on Light-Induced Solid–Liquid Phase Transition: Application to Bonding for Various Substrates, Macromol. Chem. Phys. 1900105 (2019) 1–6. doi:10.1002/macp.201900105.

[39] S. Ito, H. Akiyama, R. Sekizawa, M. Mori, M. Yoshida, H. Kihara, Light-Induced Reworkable Adhesives Based on ABA-type Triblock Copolymers with Azopolymer Termini, ACS Appl. Mater. Interfaces. 10 (2018) 32649–32658. doi:10.1021/acsami.8b09319.

[40] C.C. Corten, M.W. Urban, Repairing polymers using an oscillating magnetic field, Adv. Mater. 21 (2009) 5011–5015. doi:10.1002/adma.200901940.

[41] B.J. Adzima, C.J. Kloxin, C.N. Bowman, Externally triggered healing of a thermoreversible covalent network via self-limited hysteresis heating, Adv. Mater. 22 (2010) 2784–2787. doi:10.1002/adma.200904138.

[42] A.S. Eggeman, S.A. Majetich, D. Farrell, Q.A. Pankhurst, Size and concentration effects on high frequency hysteresis of iron oxide nanoparticles, IEEE Trans. Magn. 43 (2007) 2451–2453. doi:10.1109/TMAG.2007.894127.

[43] Z. Li, M. Kawashita, N. Araki, M. Mistumori, M. Hiraoka, Effect of Particle Size of Magnetite Nanoparticles on Heat Generating Ability under Alternating Magnetic Field, Bioceram. Dev. Appl. 1 (2011). doi:10.4303/bda/D110128.

[44] S. L. Semiatin, S. Zinn, Induction Cap Sealing and Packaging, in: C. publication Service (Ed.), Elem. Induction Heat. Des. Control. Appl., 6th ed., Electric power research institute, 2002: p. 291.

[45] R. Belouadah, D. Guyomar, B. Guiffard, J.W. Zhang, Phase switching phenomenon in magnetoelectric laminate polymer composites: Experiments and modeling, Phys.

B Condens. Matter. 406 (2011) 2821–2826. doi:10.1016/j.physb.2011.04.036.

[46] N. Hohlbein, A. Shaaban, A.M. Schmidt, Remote-controlled activation of self-healing behavior in magneto-responsive ionomeric composites, Polymer (Guildf). 69 (2015) 301–309. doi:10.1016/j.polymer.2015.04.024.

[47] T. Bayerl, M. Duhovic, P. Mitschang, D. Bhattacharyya, The heating of polymer composites by electromagnetic induction - A review, Compos. Part A Appl. Sci. Manuf. 57 (2014) 27–40. doi:10.1016/j.compositesa.2013.10.024.

[48] K.A. Houton, G.M. Burslem, A.J. Wilson, Development of solvent-free synthesis of hydrogen-bonded supramolecular polyurethanes, Chem. Sci. 6 (2015) 2382–2388. doi:10.1039/c4sc03804e.

[49] M. Shahrousvand, M.S. Hoseinian, M. Ghollasi, A. Karbalaeimahdi, A. Salimi, F.A. Tabar, Flexible magnetic polyurethane/Fe2O3 nanoparticles as organic-inorganic nanocomposites for biomedical applications: Properties and cell behavior, Mater. Sci. Eng. C. 74 (2017) 556–567. doi:10.1016/j.msec.2016.12.117.

[50] P. Jayakrishnan, M.T. Ramesan, Studies on the effect of magnetite nanoparticles on magnetic, mechanical, thermal, temperature dependent electrical resistivity and DC conductivity modeling of poly (vinyl alcohol-co-acrylic acid)/Fe3O4 nanocomposites, Mater. Chem. Phys. 186 (2017) 513–522. doi:10.1016/j.matchemphys.2016.11.028.

[51] S.J. Eichhorn, A.Dufresne, M. Aranguren, N.E. Marcovich, J.R. Capadona, S.. Rowan, C. Seder, W. Thielemans, M. Rowan, S. Renneckar, W. Gindl, S. Veigel, J. Keckes, H. Yano, K. Abe, M. Nogi, A.N. Nakagaito, A. Mangalam, J. Simonsen, A.S. Benight, A. Bismarck, L.A. Berglund, T. Peijs, Review: Current international research into cellulose nanofibres and nanocomposites, J. Mater. Sci. 45 (2010) 1–33. doi:10.1007/s10853-009-3874-0.

[52] R. Vaiyapuri, B.W. Greenland, H.M. Colquhoun, J.M. Elliott, W. Hayes, Molecular recognition between functionalized gold nanoparticles and healable, supramolecular polymer blends – a route to property enhancement, Polym. Chem.

4 (2013) 4902–4909. doi:10.1039/c3py00086a.

Supporting information

Composite polyurethane adhesives that debond-on-demand by hysteresis heating in an oscillating magnetic field.

Sara Salimi, Tahkur S. Babra, Gerald S. Dines, Stephen W. Baskerville, Wayne Hayes, and Barnaby W. Greenland

Contents

1- ^{1}H NMR and ^{13}C NMR Spectra

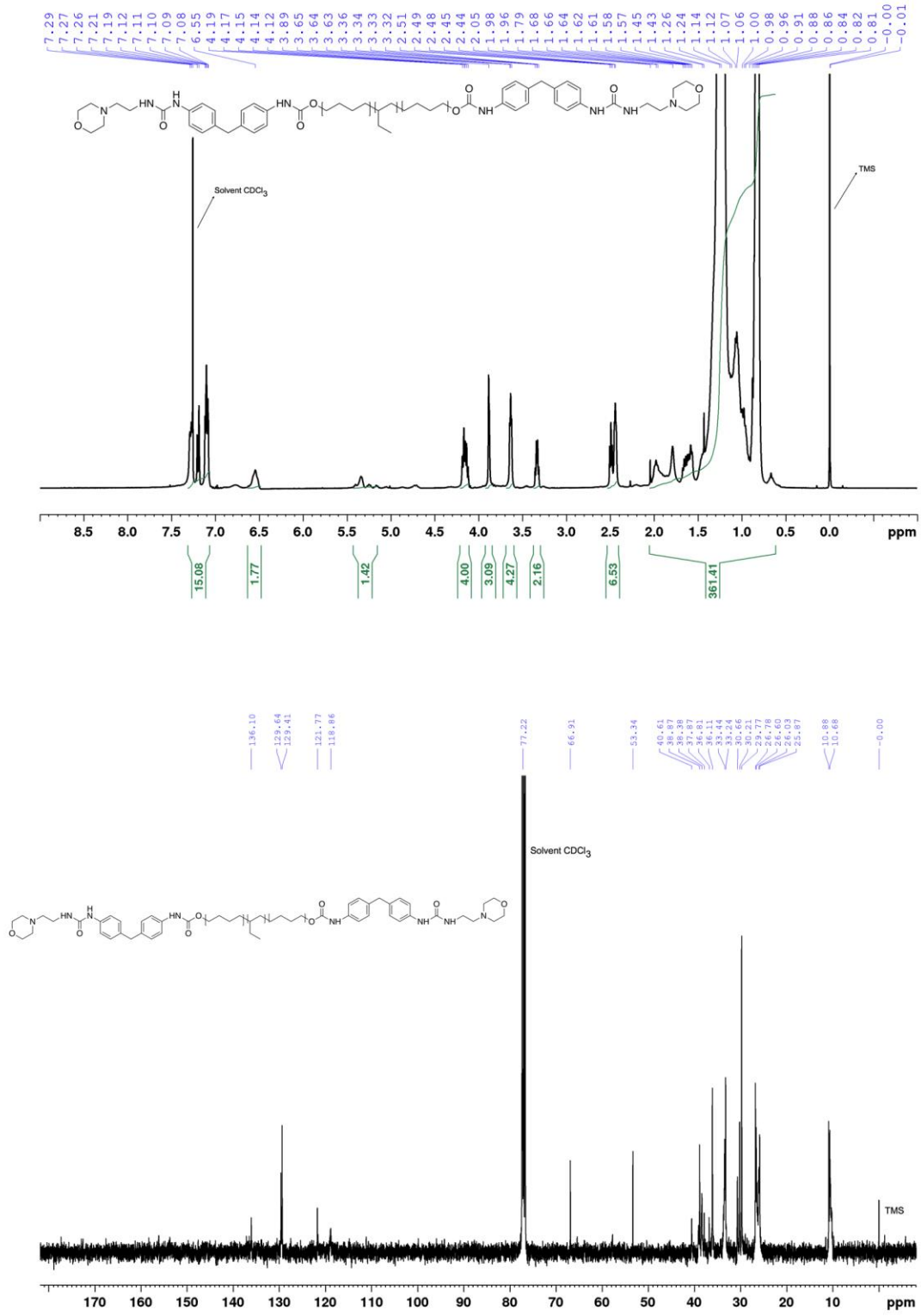

Figure S 1: NMR spectra of PU 1 in CDCl3 at 400 MHz.

2- DSC Thermograms

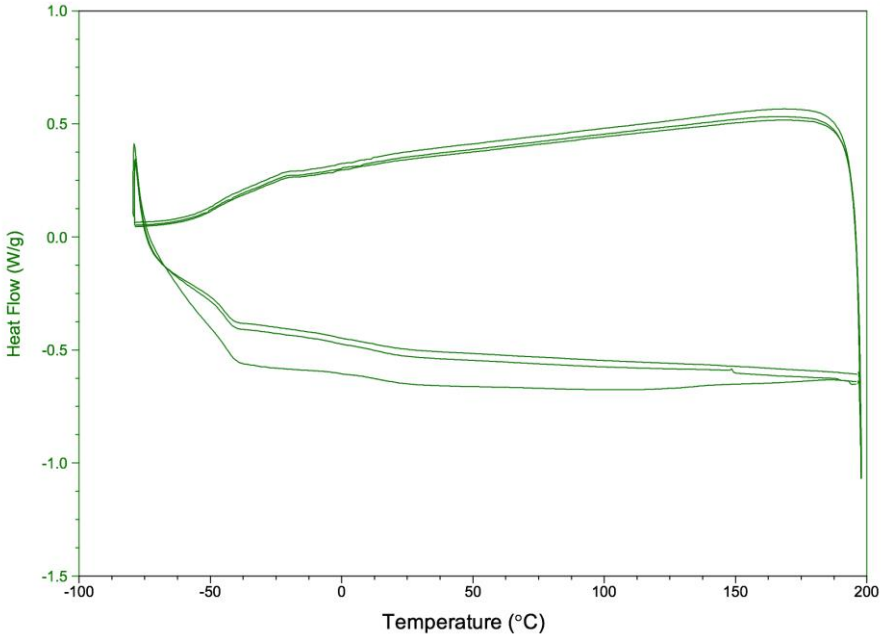

Figure S 2:The DSC experiment was carried out using Tzero aluminum pans in a DSC Q2000 instrument. 0.7 mg of the sample was heated from -80 °C to 200 °C by rate of 10 °C/min under N_2 atmosphere.

3- VT-NMR

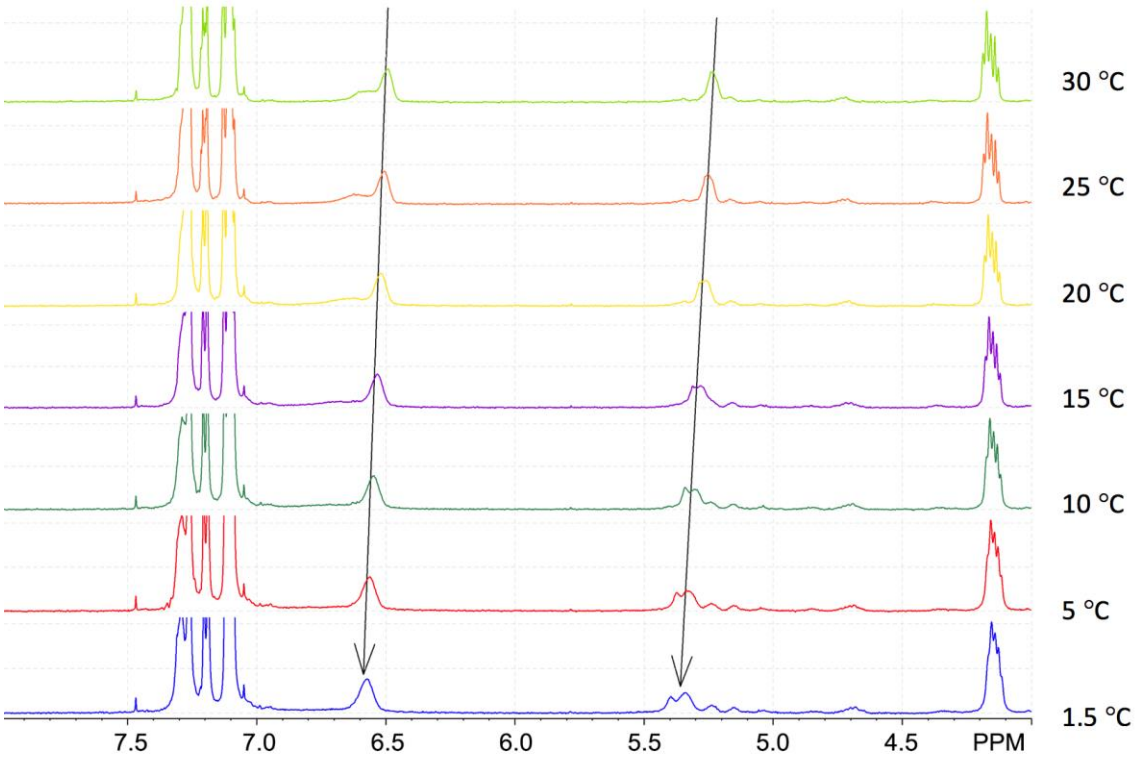

Figure S3: Partial VT-NMR (500 MHz) spectra of PU 1 showing changes in chemical shifts of NH group of urea and urethane between 1.5 and 30 ºC (arrows over signals at c. 5.4 and 6.6 ppm).

In Figure S3 arrows are pointing at the resonances representing NH groups of urea and urethane linkages. The downfield shift of these resonances results from an increase in hydrogen bonding upon decreasing the temperature.

4- **IR spectra** and **variable temperature IR spectra**

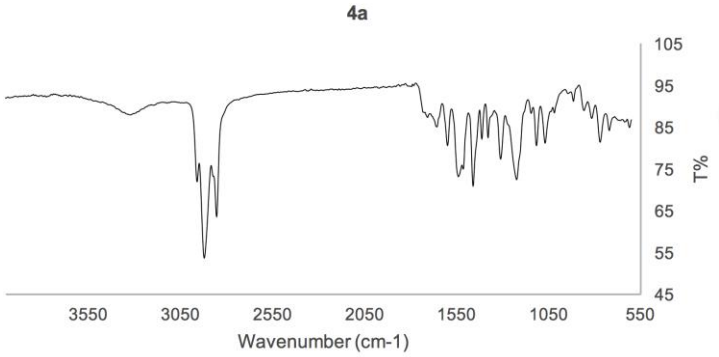

Figure S4: IR spectra of the polymer film collected using PerkinElmer Spectrum 100 FT-IR Spectrometer.

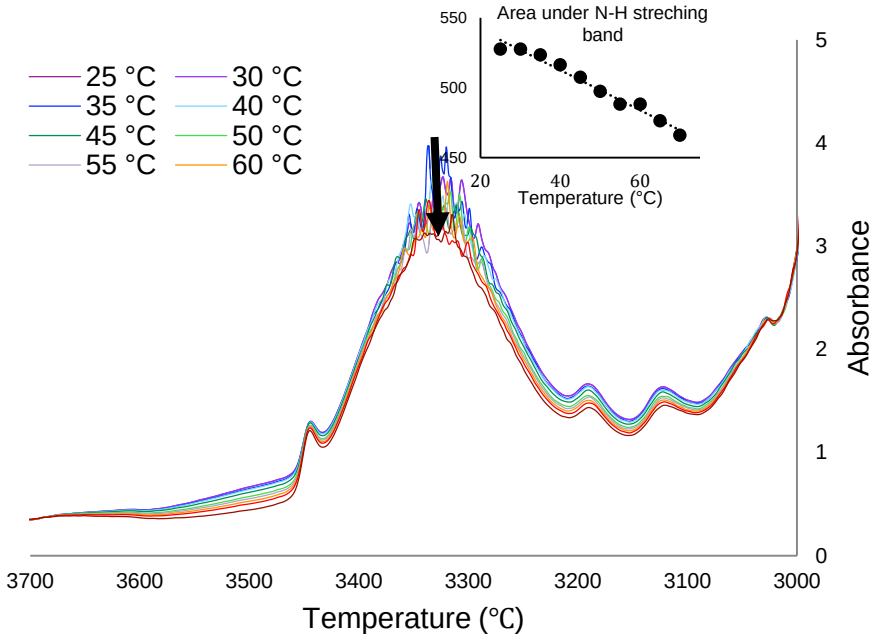

Figure S5: VT-IR Spectra of the adhesive film.

The VT-IR experiment was performed on a thin film. The sample was placed between two discs of the metal sample holder. The temperature shown are the temperature of the sample holder. The integration of the N-H peak was carried out between 3200 to 3400 cm^{-1} for each temperature. As the temperature of the sample increased, the intensity of the signal indicative of a hydrogen bonded NH (3320 cm^{-1}) decreased (≈ 14%), confirming a reduction in strength of the hydrogen bonds.[1]

5- Unprocessed images of the adhesives

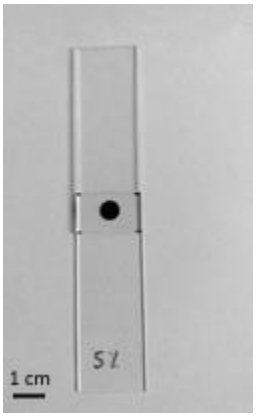

Figure S 6: Photo of a lap shear test sample.

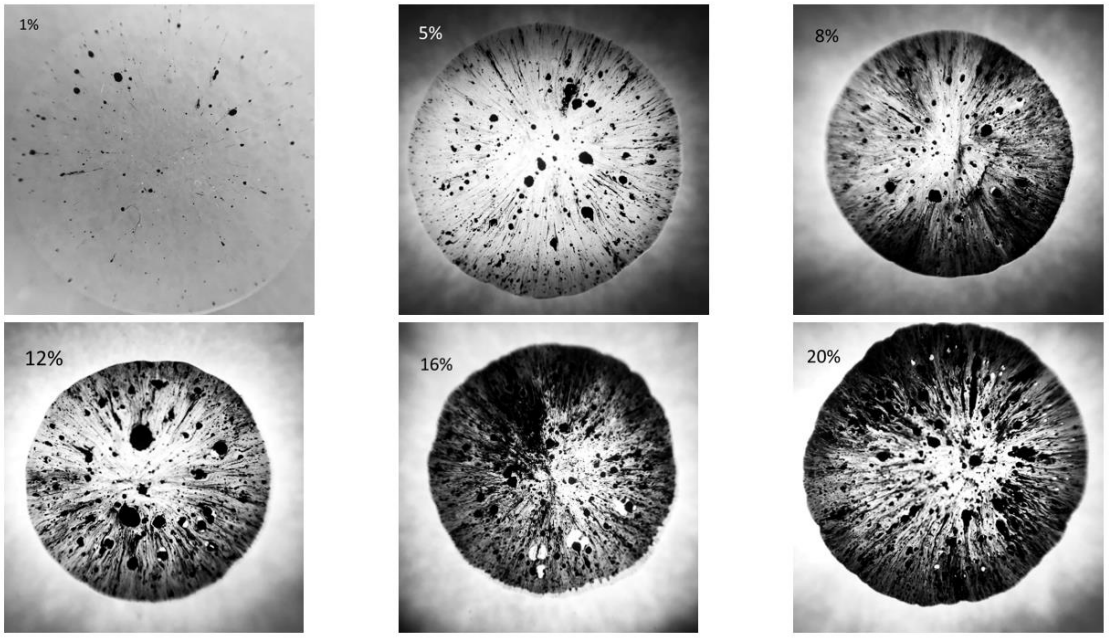

Figure S 7: Unprocessed pictures of the composite samples using macro lens and back light.

Figure S 8: Photo of dog-bone shaped samples for debonding experiment under OMF condition prior to heating in and oven.

6 - Tensile Tests

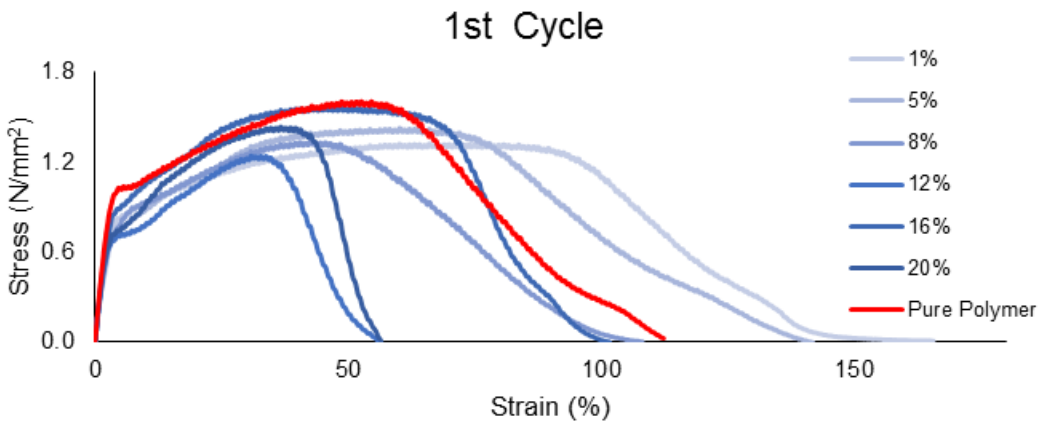

Figure S 9: Lap shear test of adhered glass slides by composites containing varying wt% filler.

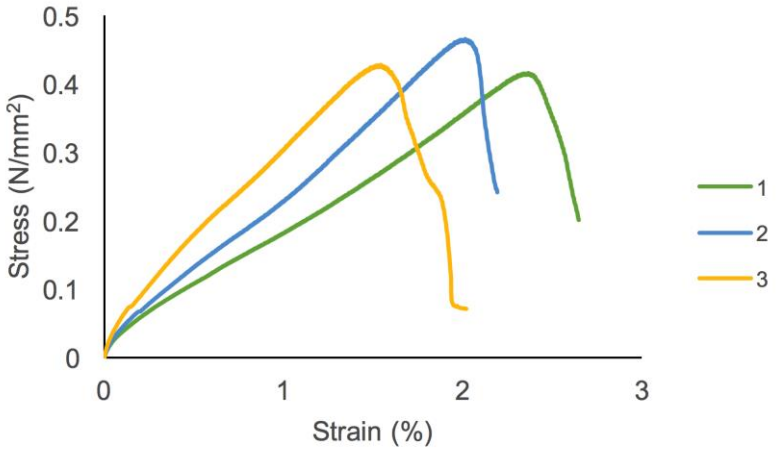

Figure S 10: Lap shear test result of three repeats of the glass slides samples adhered by the Tecbond™ hot glue.

2 mg of Tecbond™ hot glue was used to adhere two glass slides which were then tested under the same conditions as used previously for the nanocomposite materials. Samples placed between the tensiometer grips and then pulled at a speed of 1 mm/min. The above graph obtained from its mechanical behaviour.

7- GPC

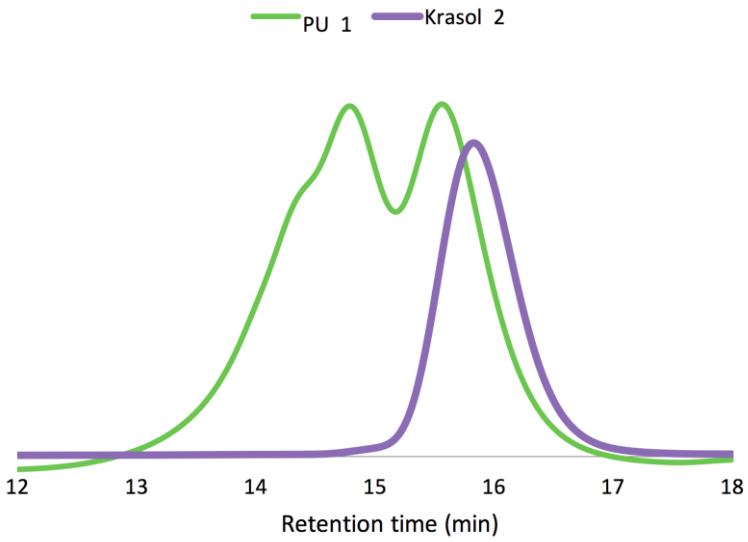

Figure S 11: GPC eluograms of the PU and the Krasol HLBH-P2000.

GPC eluograms of the PU and the starting diol (Krasol HLBH-P2000) in THF stabilised with Butylated hydroxytoluene. PU: Mn = 10300 Da, Mw = 6300 Da, Đ = 1.63. Krasol™ HLBH-P2000: Mn = 3400 Da, Mw = 3700 Da, Đ = 1.10.

8- Rheology

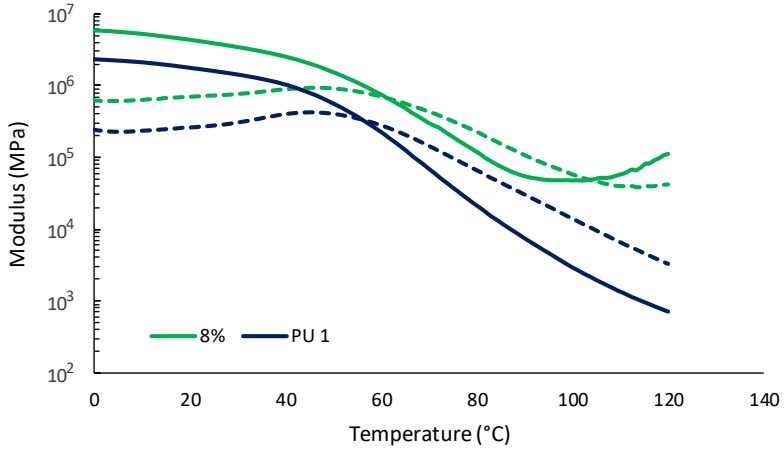

Figure S 12: Storage (solid lines) and loss (hashed lines) modulus of the 8 wt% composite (Green) and to **PU 1** (blue) between 0 and 120 °C.

9- References

[1] D.J. Skrovanek, S.E. Howe, P.C. Painter, M.M. Coleman, Hydrogen Bonding in Polymers: Infrared Temperature Studies of an Amorphous Polyamide, Macromolecules. 18 (1985) 1676–1683.